Processing and Application of Ceramics 14 [2] (2020) 173–180
https://doi.org/10.2298/PAC2002173S

Preparation and properties of $Zr_2WP_2O_{12}$ with negative thermal expansion without sintering additives

Xin Wei Shi[1,*], Qiang Zhou[1], Xiaosheng Yan[1], Xingrui Li[2], Bailin Zhu[3]

[1]*School of Physics and Microelectronics, Zhengzhou University, Henan 450001, PR China*
[2]*School of Materials Science and Engineering, Zhengzhou University, Henan 450001, PR China*
[3]*State Key Laboratory of Refractories and Metallurgy, Wuhan University of Science and Technology, Wuhan 430081, PR China*

Received 20 January 2020; Received in revised form 22 April 2020; Accepted 1 May 2020

Abstract

Zirconium tungsten phosphate ($Zr_2WP_2O_{12}$ denoted as ZWP) is a negative thermal expansion material which can be used as filler in controlling the thermal expansion coefficient of other materials. In this study, dense ZWP ceramics without any additives was prepared via solid-state reaction method, by milling the as-synthesized powder for different times and sintering at 1300 °C. The influence of the milling time, i.e. reduced particle sizes, on properties of the $Zr_2WP_2O_{12}$ was investigated. The obtained samples were characterized by X-ray diffraction (XRD) method, scanning electron microscopy (SEM), thermal mechanical analysis (TMA), Raman spectroscopy and Vickers hardness tester. The results showed that the milled powders have high crystallinity with single phase orthorhombic structure. The ZWP ceramics exhibits NTE property with high density. With the increase of milling time the coefficient of thermal expansion changed from -2.607×10^{-6} 1/K to -3.914×10^{-6} 1/K. In addition, the grain sizes decrease and the relative density and HV hardness of the obtained ceramics increase confirming that grinding is an effective method to improve the performance of ZWP ceramics.

Keywords: *$Zr_2WP_2O_{12}$, negative thermal expansion, particle size, milling time, sintering*

I. Introduction

As it is well known, most of the materials in nature expand when heated. However, different materials may display different coefficient of thermal expansion (CTE). These differences between components of a device are known as thermal mismatch, which have been recognized as a serious problem in many fields, such as road surfaces, railroad tracks and bridges, thin films and other high-end applications (e.g. aerospace field) [1–6]. Reportedly, thermal mismatch between different materials may lead to a series of problems, such as cracking of coatings or layers, device failures, device precision reduction and service life shortening of devices. This phenomenon is especially evident in electronics and optoelectronic devices [7,8]. Fortunately, in nature there is another kind of materials called negative thermal expansion (NTE) materials, which contract upon heating instead of expanding compared with most materials. Due to the negative expanding property, they can be used to control CTE of other materials. For example, they can be combined with other material to make composites with zero or controlled thermal expansion [1,9–11]. During the last twenty years, the field of NTE materials has expanded rapidly since Sleight's group found that ZrW2O8 has large isotropic NTE behaviour between the temperature range of 0.3–1050 K in 1996 [12,13]. From then on, NTE materials began to attract attention of many researchers and formed a specialized field of research [1]. ZrW_2O_8, ZrV_2O_7 and $Sc_2W_3O_{12}$ are the typical representatives. Many researches have been focused on ZrW_2O_8 for its large isotropic CTEs. The structure of ZrW_2O_8 is composed of corner-sharing ZrO_6 octahedra and WO_4 tetrahedra, with each ZrO_6 connected to six WO_4 units [1]. Due to its cubic structure, ZrW_2O_8 expands and shrinks equally in all axes, with large α_1 value of -9.1×10^{-6} 1/K [1,9,14]. However, this material may undergo a phase transition from

*Corresponding author: tel: +86 13837167882,
e-mail: *Shixw@zzu.edu.cn*

α-ZrW_2O_8 to β-ZrW_2O_8 at about 420 K and α-ZrW_2O_8 to γ-ZrW_2O_8 at the pressure of about 0.2 to 0.3 GPa [1,8,9,14–17]. Correspondingly, the CTE value changes to -4.9×10^{-6} 1/K [8,10] and -1×10^{-6} 1/K [18–20], respectively. This kind of phase transition induced by temperature or pressure is undesirable and maybe fatal in important application areas. For example, device in aerospace fields using ZrW_2O_8 as NTE filler may not work properly or crack due to the sharp change of CTE. Thus, cataclysmic or fatal events may happen [8]. From this point of view, the stability of thermal expansion is very important.

Based on these backgrounds, Isobe *et al.* [8,9] specifically examined zirconium tungsten phosphate $Zr_2(WO_4)(PO_4)_2$ or $Zr_2WP_2O_{12}$ (hereafter denoted as ZWP) as a novel NTE material. The crystal structure of ZWP at room temperature was assigned to orthorhombic space group *Pnca* by Evans *et al*. [21]. ZWP contains ZrO_6 octahedra sharing corners with four PO_4 tetrahedra and two WO_4 tetrahedra [8,22]. The NTE behaviour of ZWP material mainly derives from the bridging O atoms' transverse motions or the coupled rotation between the octahedral and tetrahedral [8,23]. ZWP is stable at all temperatures from at least as low as −50 °C to at least as high as 1150 °C [8,24]. The structure, preparation process and properties of ZWP have been reported, e.g. Wilkinson [22,25], Evans [21,26], Isobe [9], Martinek [27], and so on. Evans *et al*. [26] measured the CTE of ZWP by X-ray diffraction and dilatometric method. The mean linear CTEs were -3×10^{-6} 1/K and -6×10^{-6} 1/K, respectively. Due to its attractive CTE, cheap raw material and stability in large temperature range, ZWP can be used as a good filler to make composites with zero or controllable CTE [8,15]. However, there have been no results reported about the effect of ZWP particle sizes on its properties to date. Particle size may greatly influence the material properties. For example, small particle sizes will improve mixing [1]. Reportedly, small particles may reduce agglomeration and easily disperse uniformly in matrix [1,10]. Interaction between filler and matrix can be improved when filler particle size decreases or specific surface area increases [10]. Sharma *et al.* [28] reported that NTE ZrW_2O_8 filler with nanoparticles can improve the mechanical strength of polyimide. NTE materials with small or even nano-sized particles can be used as pure phase or used to control the CTE of other materials. Hence, it is interesting to explore the effect of ZWP particle sizes on its own performance or its composites.

In this study, ZWP powder was prepared by a solid-state reaction method without sintering additives. To reduce the particle sizes, the synthesised ZWP powder was ball milled at different times. ZWP ceramics with different particle sizes were pressed by cold pressing and sintered at 1300 °C. The structure and morphologies of the ZWP particles were examined and its effects on the thermal and mechanical properties of the ZWP ceramics were studied.

II. Experimental

ZWP powder was prepared by solid-state reaction method using stoichiometric amounts of ZrO_2 (purchased from Tianjin Guangfu Fine Chemical Research Institute, China), WO_3, and $NH_4H_2PO_4$ (purchased from Tianjin Kermel Reagent Co., Ltd. China) with purity of more than 99.0% and average particle size of about 1.5 μm, 15 μm and 1 mm, respectively. A molar ratio of Zr : W : P = 2 : 1 : 2 was maintained during the preparation process. The starting materials were ground in an agate mortar and mixed thoroughly. The mixture was heated to 1200 °C for 4 h in a crucible and slowly cooled in furnace to room temperature. Then the mixture was ball mixed using a planet lapping machine for different time (2, 12, 24, 48, 72, 96 h) in ethanol. The powder mixture was heated for 6 h at 80 °C to remove the ethanol after the milling process. The resulting powders were then uniaxially cold pressed at 30 MPa to form disks (10 mm in diameter and 4 mm in height). The disks were then sintered at 1300 °C for 4 h to obtain ZWP ceramics for thermal and mechanical properties tests.

A Bruker D8 Advance Diffractometer was used to carry out the XRD measurements. The morphologies of the ZWP powders were obtained on a scanning electron microscope (SEM). The particle sizes of the milled ZWP powders were calculated from SEM images using a Nano-Measurer program (1.2 version). The mean linear CTEs of the ZWP ceramics were obtained on a dilatometer (LINSEIS DIL L76, LINSEIS Instruments Ltd., Germany). The Archimedes technique was used to determine the relative densities of the sintered ZWP ceramics. The HV hardness of the ZWP ceramics was tested by a Vickers hardness tester with a load of 9.8 N. Each sample was tested 10 times at different points and then the average value was calculated as the final HV hardness.

III. Results and discussion

3.1. XRD and Raman analyses

Figure 1 shows the XRD patterns of the milled ZWP powders. It can be seen that the XRD pattern of the ZWP powder milled for 96 h (Fig. 1b) coincides well with the orthorhombic phase with space group *Pnca* (No. 60). The XRD patterns of the samples milled for different times keep unchanged and they were almost the same, which demonstrates that the orthorhombic structure is maintained with different milling times. Thus, the results confirm that single phase orthorhombic ZWP was successfully synthesized by solid-state reaction method. From the graph, the main peaks at about 22.5° and 23.7° move towards right slightly with increasing milling time, which can be seen obviously from the insert in Fig. 1a. This could be confirmation of continuous incorporation of some smaller cations in the lattice of the final product. More detailed research will be

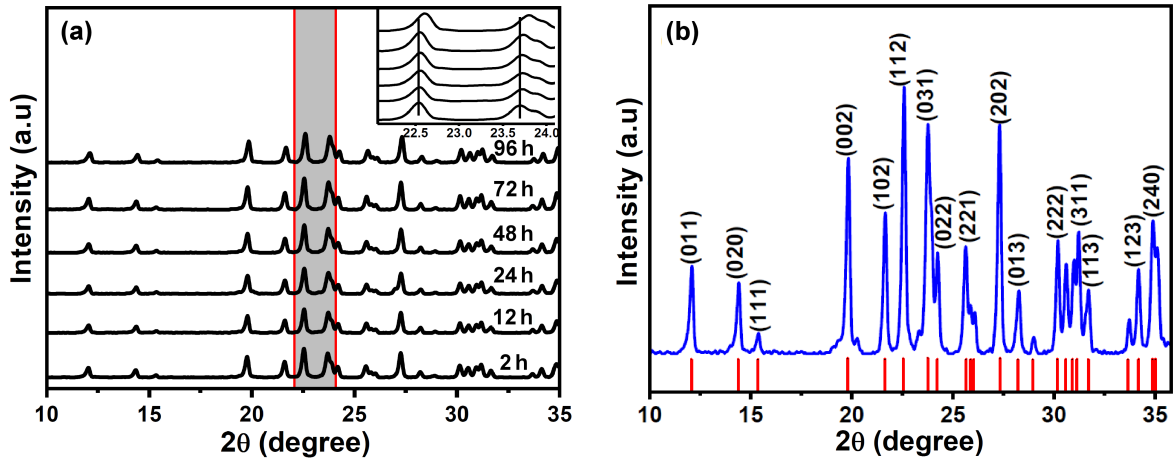

Figure 1. XRD patterns of: a) the obtained ZWP powders milled for different time and b) powder milled for 96 h (compared with the standard PDF card)

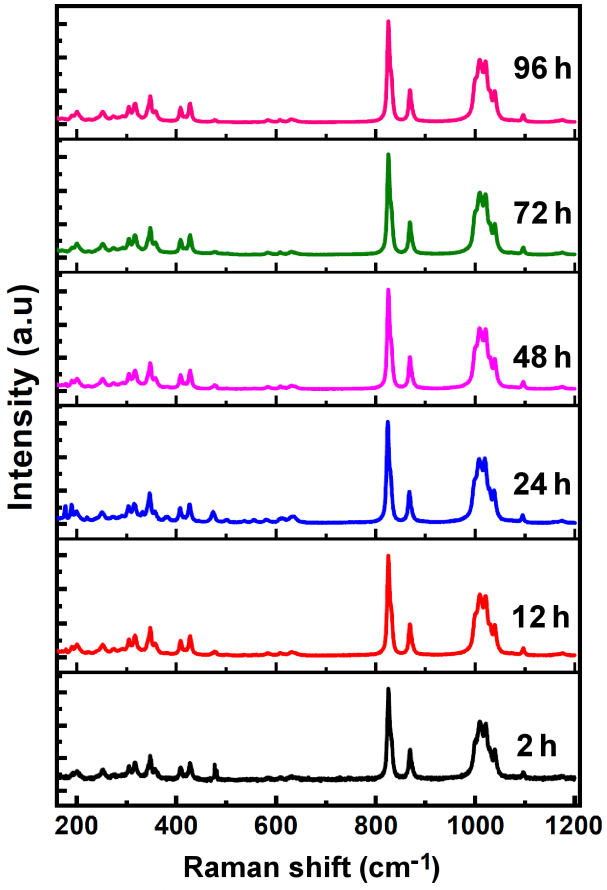

Figure 2. Raman spectra of the obtained ZWP powders milled for different times

carried out later. On the other hand, according to the Bragg equation, when diffraction angles move to higher values, the interplanar spacing decreases and this may influence the thermal expansion of the final product.

Figure 2 gives the Raman spectra of the ZWP synthesized by solid-state reaction and milled for different times. It is obvious that the Raman spectra of the ZWP powders milled for different times are almost the same. ZWP comprises ZrO_6 octahedra sharing corners with two WO_4 tetrahedra and four PO_4 tetrahedra [21,22]. The Raman modes at about 1040 to 900 cm^{-1}, 900 to 700 cm^{-1} and 475 to 305 cm^{-1} can be assigned to the symmetric stretching vibration (ν_1), asymmetric stretching vibration (ν_3) and bending vibrations ($\nu_2 + \nu_4$) of WO_4 tetrahedra, respectively [29]. The lower Raman modes, below 300 cm^{-1}, can be ascribed to the lattice modes arising from Zr atom motions, translational and vibrational motions of WO_4 tetrahedral and ZrO_6 octahedra [30,31]. P–O stretching vibration can be observed at high Raman modes. The bands at about 1174 and 1095 cm^{-1} may be attributed to the symmetric stretching vibration (ν_1) and the asymmetric stretching vibration (ν_3) of PO_4 tetrahedra, respectively [32,33]. The Raman spectra confirmed the presence of ZrO_6 octahedra and WO_4 and PO_4 tetrahedra. Table 1 gives the Raman bands positions of the obtained ZWP powders and the vibrations of PO_4 and WO_4 tetrahedra.

Table 1. Raman band positions of ZWP

Band position [cm^{-1}]	Assignment
1174, 1097	ν_1 (PO_4)
1039 ,1021, 1011, 872, 828	ν_1 (WO_4)
634, 612, 583, 475, 428, 408	$\nu_2 + \nu_4$ (PO_4)
347, 317, 305	$\nu_2 + \nu_4$ (WO_4)

3.2. SEM analyses

SEM micrographs of the ZWP powders were shown in Fig. 3. It can be seen obviously that the particle sizes are reduced with the increased milling time. From Fig. 3 we can also see that the morphologies of the particles changed with the milling time. For low milling times (2, 12, 24 and 48 h), particles of all powders are nearly spherical. Because of large surface energy, these spherical particles may easily agglomerate. However, for longer milling times (72 and 96 h), cone granular particles appear and the size decreases. These kinds of particles may become less agglomerated.

The average particle sizes of the obtained ZWP powders were calculated using a Nano-Measurer program

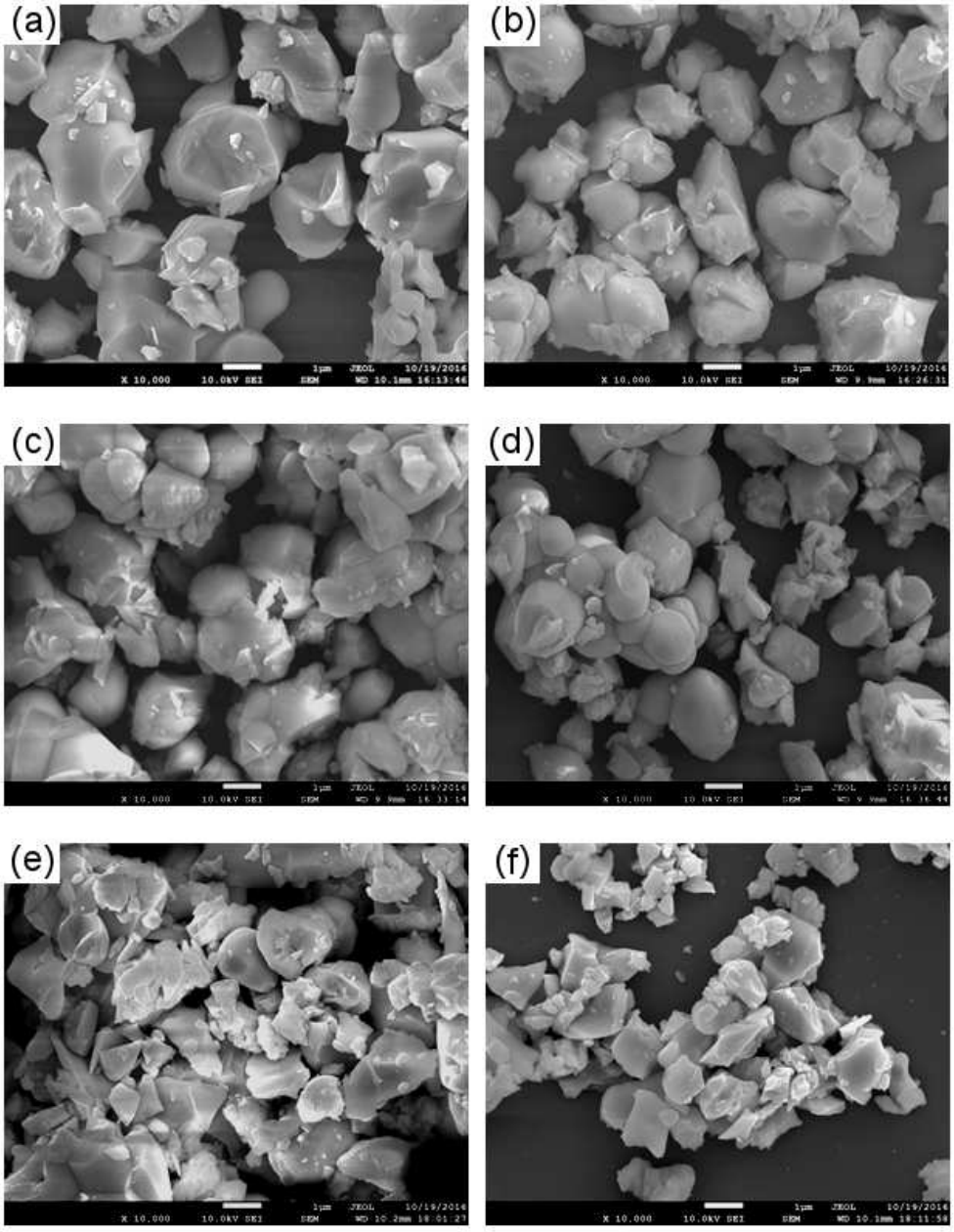

Figure 3. SEM images of the ZWP powders milled for different times: a) 2 h, b) 12 h, c) 24 h, d) 48 h, e) 72 h and f) 96 h

(1.2 version) [34] according to SEM photographs; more than 200 particles were chosen for the calculation. We can see from Fig. 4 that the average particle sizes decrease apparently with the milling time increasing. Thus, the average particle size decreases from 2700 to about 650 nm when milling time increases from 2 to 96 h. It is well known that small particles can be more easily dispersed in the matrix [10]. The insert in Fig. 4 illustrates the particle size distribution of the powders milled for 96 h, which proved that the particle size mainly distributes in the range from 550 to 650 nm.

3.3. Influence of particle size on relative density

The Archimedes technique was used to estimate relative densities of the ZWP ceramics (Fig. 5). With the milling time increasing, the experimental density value increase (the insert), indicating that densities were affected by milling time. This may be due to the fact that with milling time increasing, the particle sizes decrease and become less agglomerated, which lead to the high density of the ZWP ceramics. The lowest relative density of the obtained ZWP ceramics is about 81.5% of their theoretical density. With the milling time prolonging, the relative density increases. When the milling time was 96 h, the relative density of the obtained ZWP ceramics reached 95.4% of their theoretical density. Compared with the result published by Isobe *et al.* [9], in which the relative density of ZWP ceramics without MgO additive is about 60%, the result in our case is pretty good.

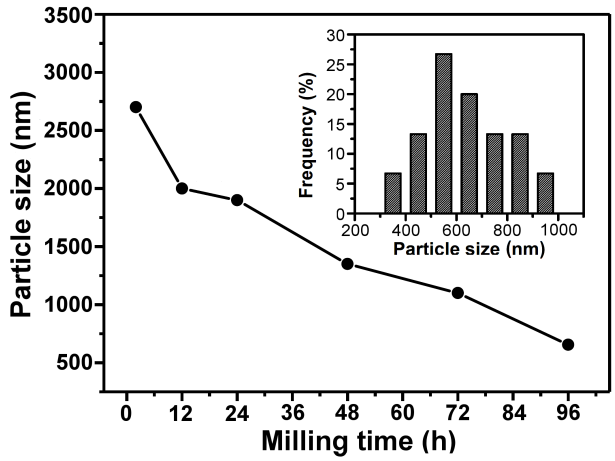

Figure 4. ZWP average particle sizes determined by Nano-Measurer program (inset shows the size distribution of the powders milled for 96 h)

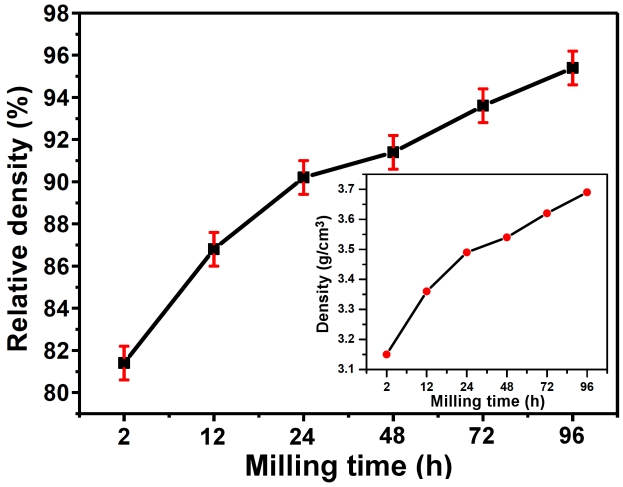

Figure 5. Dependence of the relative density on milling time

Figure 6 presents the SEM morphologies of the ZWP ceramics obtained from the powders milled for 2 and 96 h, respectively. It can be seen that the particle size in the ZWP ceramics obtained from the powder milled for 96 h is comparatively smaller, which leads to enhanced densification of the ceramics, as identified in Fig. 6 with green circles. The ZWP ceramics obtained from the powder milled for 2 h has larger grains and more pores which cause the reduction of the relative density [8]. Hence, the relative density of the obtained samples increases with the increase of the milling time.

3.4. Influence of particle size on CTEs

CTEs of the sintered ceramics prepared from the ZWP powders milled for different times were measured using a TMA and calculated according to Eq. 1 [35–38]:

$$\alpha = \frac{1}{L_0} \cdot \frac{\Delta L}{\Delta T} \tag{1}$$

In the formula, L_0 represents the initial length of the sample and $\Delta L/\Delta T$ is the length change caused by temperature variation.

Figure 7 illustrates $\Delta L/L_0$ (the relative length changes) of the obtained ZWP ceramics in temperature interval from 298 to 800 K. It can be seen that all ZWP ceramics shrank with increasing temperature, i.e. exhibit negative thermal property. With the milling time increasing (from 2 to 96 h), the CTE value of the obtained ZWP ceramics changes from -2.607×10^{-6} 1/K to -3.914×10^{-6} 1/K. It is reported by Evans *et al.* [21] that the mean linear CTEs of ZWP tested by XRD and dilatometer method were -3×10^{-6} 1/K and -6×10^{-6} 1/K, respectively. Isobe *et al.* [9] prepared ZWP ceramics using 0.5 wt.% of MgO as a sintering additive. The CTE was tested by a thermomechanical analyser from 303 K to 873 K and its value was -3.4×10^{-6} 1/K. In our case, the ZWP samples were obtained without any additive and the CTE value can reach -3.914×10^{-6} 1/K. This proves that extended grinding time is an effective method to reduce CTE of ZWP. It is worth mentioning that the curves in Fig. 7 are smooth and no steep slopes appear, which fully proves that the

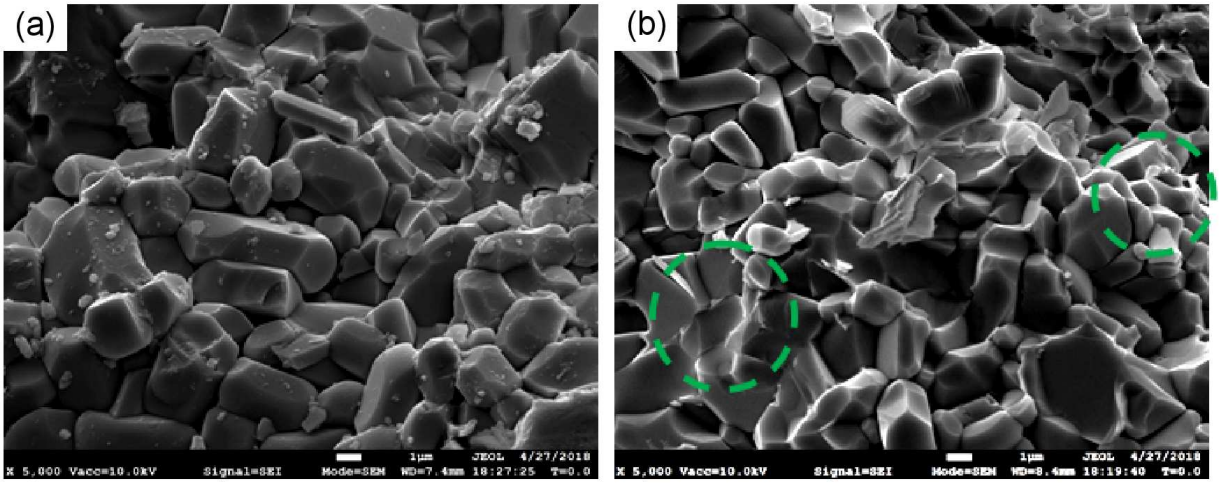

Figure 6. SEM images of the ZWP ceramics obtained from powders milled for: a) 2 h and b) 96 h

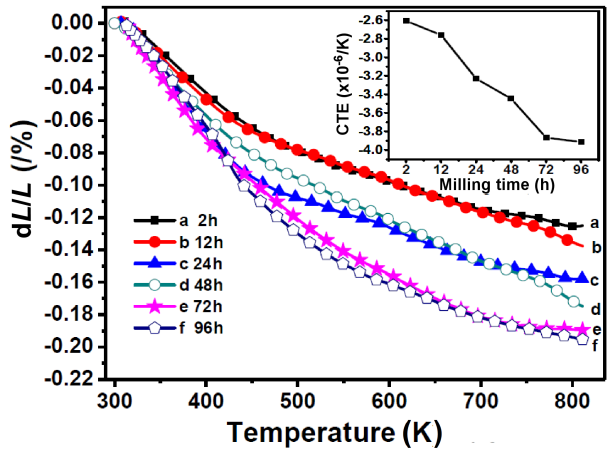

Figure 7. Relative length change of ZWP ceramics with different milling times

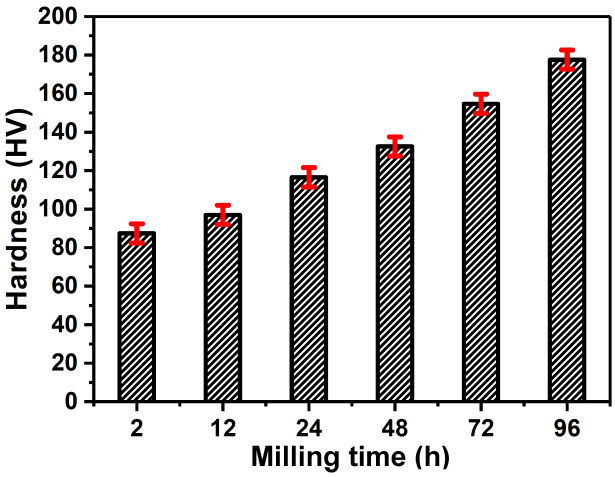

Figure 8. Relationship between the HV hardness of ZWP and milling time

prepared ZWP is stable in the range of testing temperature and no new phase appears [8,9]. The result agrees with that deduced from the XRD analysis.

The CTE of the materials is also related to the relative density, i.e. amount of porosity. It is reported that the porosities may accommodate the internal thermal expansion of material, which lead to the CTE reduction [39]. In our case, the particle sizes decrease with the milling time increasing. The smaller the particles are, the denser of the ZWP ceramics will be obtained, which is consistent with the results from Figs. 5 and 6. As a result, the CTE value reduced with the milling time increasing.

3.5. Influence of particle size on hardness

The hardness of the obtained ZWP ceramics was measured by a Vickers hardness tester with a 9.8 N load and kept for 30 s. Each reported HV value of each sample is an average of at least 10 measurements. Figure 8 portrays the HV hardness of the ZWP ceramics changed with the milling time. It can be seen that with the milling time increasing, the HV hardness of the ceramics increases. This may be due to the fact that with the milling time increasing, the relative density of the ZWP ceramics increased (Fig. 5), which will lead to the densification of the samples. In general, materials with high density will have high hardness. So, the hardness of the obtained ZWP samples enhanced with the milling time increasing. However, the hardness of our samples is lower compared to the data published by Iosbe *et al.* [9]. They prepared ZWP ceramics by using sintering additive and obtained also high hardness. We think that in their case the sintering additive (0.5 wt.% of MgO) may act as a kind of strengthening phase or a kind of bonding medium between ZWP particles, which lead to high hardness. Hence, adding sintering additive and at the same time prolonging the powders milling time may be a good combination method to improve the properties of ZWP ceramics. Related research will be carried out in the future.

IV. Conclusions

Zirconium tungsten phosphate (ZWP) ceramics with high relative density and acceptable CTE were obtained from solid-state synthesized powders and without any sintering additives. By solid-state reaction method and grinding, single phase orthorhombic ZWP powders were obtained and their average particle size decreases with the milling time increasing. Prolonging the powder milling time (up to 96 h) also improved the performance of the ZWP ceramics. The obtained ZWP ceramics exhibit NTE property. The CTE of the ZWP ceramics obtained from the ZWP powder milled for 96 h is -3.914×10^{-6} 1/K. Both the relative density and the hardness increase with the milling time and when the milling time is 96 h, the relative density of the obtained ZWP ceramics is 95.4% of its theoretical density. These results suggest that extending the grinding time is an effective method to improve the performance of ZWP ceramics.

Acknowledgement: This work was supported by the following projects: National Science Foundation of China (No. 11574276, 11874328), Henan Provincial Natural Science Foundation of China (No. 182300410192) and The Foundation and Frontier Technology Research Programs of Henan Province (No. 152300410038).

References

1. C. Lind, "Two decades of negative thermal expansion research: Where do we stand?", *Materials*, **5** (2012) 1125–1154.
2. J. Qi, J. Ba, H. Li, J. Lin, X. Zheng, J. Cao, J. Feng, "β-$LiAlSiO_4$ reinforced Cu composite interlayer for brazing C/C composites and Nb", *Vacuum*, **172** (2020) 109102.
3. Z.C. Wang, J.C. Lin, P. Tong, M.G. Kong, X.K. Zhang, C. Yang, W.H. Song, Y.P. Sun, "Tunable thermal expansion in zinc-bonded composites: $Zn/Si/Zn_{0.75}Sn_{0.2}Mn_{0.05}NMn_3$", *Scripta Mater.*, **177** (2020) 166–171.
4. J. Zygmuntowicz, M. Piatek, A. Miazga, K. Konopka, W.

Kaszuwara, "Dilatrometric sintering study and characterization of alumina-nickel composites", *Process. Appl. Ceram.*, **12** [2] (2018) 111–117.
5. E.M. Parsons, "Lightweight cellular metal composites with zero and tunable thermal expansion enabled by ultrasonic additive manufacturing: Modeling, manufacturing, and testing", *Compos. Struct.*, **223** (2019) 110656.
6. J. Ba, X. H. Zheng, R. Ning, J.H. Lin, J.L. Qi, J. Cao, W. Cai, J.C. Feng, "C/SiC composite-Ti6Al4V joints brazed with negative thermal expansion ZrP_2WO_{12} nanoparticle reinforced AgCu alloy", *J. Eur. Ceram. Soc.*, **39** (2019) 755–761.
7. X.-S. Liu, F.-X. Cheng, J.-Q. Wang, W.-B. Song, B.-H.Yuan, E.-J. Liang, "The control of thermal expansion and impedance of Al-$Zr_2(WO_4)(PO_4)_2$ nano-cermets for near-zero-strain Al alloy and fine electrical components", *J. Alloys Compd.*, **553** (2013) 1–7.
8. X. Shi, H. Lian, R. Qi, L. Cui, N. Yao, "Preparation and properties of negative thermal expansion $Zr_2WP_2O_{12}$ powders and $Zr_2WP_2O_{12}$/TiNi composites", *Mater. Sci. Eng. B*, **203** (2016) 1–6.
9. T. Isobe, T. Umezome, Y. Kameshima, A. Nakajima, K. Okada, "Preparation and properties of negative thermal expansion $Zr_2WP_2O_{12}$ ceramics", *Mater. Res. Bull.*, **44** (2009) 2045–2049.
10. L.C. Kozy, M.N. Tahir, C. Lind, W. Tremel, "Particle size and morphology control of the negative thermal expansion material cubic zirconium tungstate", *J. Mater. Chem.*, **19** (2009) 2760–2765.
11. H. Hayun, R. Wolf, C. Barad, Y. Gelbstein, "Thermal shock resistant solid oxide fuel cell ceramic composite electrolytes", *J. Alloys Compd.*, **821** (2020) 153490.
12. T.A. Mary, J.S.O. Evans, T. Vogt, A.W. Sleight, "Negative thermal expansion from 0.3 to 1050 Kelvin in ZrW_2O_8", *Science*, **272** (1996) 90–92.
13. H. Wang, M.J. Yang, M. Chao, J. Guo, X. Tang, Y. Jiao, E. Liang, "Negative thermal expansion properties of $Cu_{1.5}Mg_{0.5}V_2O_7$", *Ceram. Int.*, **45** (2019) 9814–9819.
14. J.S.O. Evans, Z. Hu, J.D. Jorgensen, D.N. Argyriou, S. Short, A.W. Sleight, "Compressibility, phase transitions, and oxygen migration in zirconium tungstate, ZrW_2O_8", *Science*, **275** (1997) 61–65.
15. H. Watanabe, J. Tani, H. Kido, K. Mizuuchi, "Thermal expansion and mechanical propreties of pure magnesium containing zirconium tungsten phosphate particles with negative thermal expansion", *Mater. Sci. Eng. A*, **494** (2008) 291–298.
16. H. Wu, P. Badrinarayanan, M.R. Kessler, "Effect of hydrothermal synthesis conditions on the morphology and negative thermal expansivity of zirconium tungstate nanoparticles", *J. Am. Ceram. Soc.*, **95** (2012) 3643–3650.
17. C. Lind, M.R. Coleman, L.C. Kozy, G.R. Sharma, "Zriconium tungstate/polymer nanocomposites: Challenges and opportunities", *Phys. Status Solidi B*, **248** (2011) 123–129.
18. P. Badrinarayanan, Md. Imteyaz Ahmad, M. Akinc, M.R. Kessler, "Synthesis, processing, and characterization of negative thermal expansion zirconium tungstate nanoparticles with different morphologies", *Mater. Chem. Phys.*, **131** (2011) 12–17.
19. J.-I. Tani, M. Takahashi, H. Kido, "Fabrication and thermal expansion properties of ZrWO/ZrWPO composites", *J. Eur. Ceram. Soc.*, **30** (2010) 1483–1488.
20. A.W. Sleight, "Isotropic negative thermal expansion", *Annu. Rev. Mater. Sci.*, **28** (1998) 29–43.
21. J.S.O. Evans, T.A. Mary, A.W. Sleight, "Structure of $Zr_2(WO_4)(PO_4)_2$ from powder X-ray data: Cation ordering with no superstructure", *J. Solid State Chem.*, **120** (1995) 101–104.
22. M. Cetinkol, A.P. Wilkinson, "Pressure dependence of negative thermal expansion in $Zr_2(WO_4)(PO_4)_2$", *Solid State Commun.*, **149** (2009) 421–424.
23. J.Z. Tao, A.W. Sleight, "The role of rigid unit modes in negative thermal expansion", *J. Solid State Chem.*, **173** (2003) 442–448.
24. G.A. Merkel, *Negative Thermal Expansion Materials Including Method of Preparation and Uses Therefor*, United State Patent No. 6,187,700 B1, 2001.
25. M. Cetinkol, A.P. Wilkinson, C. Lind, "In situ high-pressure synchrotron X-ray diffraction study of $Zr_2(WO_4)(PO_4)_2$ up to 16 GPa", *Phys. Rev. B*, **79** [22] (2009) 224118.
26. J.S.O. Evans, T.A. Mary, A.W. Sleight, "Negative thermal expansion in a large molybdate and tungstate family", *J. Solid State Chem.*, **133** (1997) 580–583.
27. C.A. Martinek, F.A. Hummel, "Subsolidus equilibria in the system ZrO_2-WO_3-P_2O_5", *J. Am. Ceram. Soc.*, **53** (1970) 159–161.
28. G.R. Sharma, C. Lind, M.R. Coleman, "Preparation and properties of polyimide nanocomposites with negative thermal expansion nanoparticle filler", *Mater. Chem. Phys.*, **137** (2012) 448–457.
29. F. Li, X. Liu, W. Song, B. Yuan Y. Cheng H. Yuan F. Cheng M. Chao, E. Liang, "Phase transition, crystal water and low thermal expansion behavior of $Al_{2-2x}(ZrMg)_xW_3O_{12} \cdot n(H_2O)$", *J. Solid State Chem.*, **218** (2014) 15–22.
30. J. Wang, Q. Chen, W. Feng, E. Liang, "Rapid synthesis and Raman spectroscopic study of the negative thermal expansion material of $A(WO_4)_2$ (A = Zr^{2+}, Hf^{2+})", *Optik*, **124** (2013) 335–338.
31. J. Wang, Q. Chen, W. Feng, E. Liang, "Study on synthesis and property of $Zr_{1-x}Hf_xW_2O_8$", *Optik*, **127** [5] (2016) 2837–2839.
32. M. Orlova, L. Perfler, M. Tribus, P. Salnikov, B. Glorieux, A. Orlova, "Temperature induced phase transition of $CaMn_{0.5}Zr_{1.5}(PO_4)_3$ phosphate", *J. Solid State Chem.*, **235** (2016) 36–42.
33. R.L. Frost, R. Scholz, L. Wang, "Vibrational spectroscopic study of the phosphate mineral kryzhanovskite and in comparison with reddingite-implications for the molecular structure", *J. Mol. Struct.*, **1118** (2016) 203–211.
34. Y. Shi, Y. Wang, D. Wang, B. Liu, Y. Li, L. Wei, "Synthesis of hexagonal prism (La,Ce,Tb)PO_4 phosphors by precipitation method", *Cryst. Growth Des.*, **12** (2012) 1785–1791.
35. Y. Guan, D. Wang, G. Song, G. Dang, C. Chen, H. Zhou, X. Zhao, "Novel soluble polyimides derived from 2,2'-bis[4-(5-amino-2-pyridinoxy)phenyl] hexafluoropropane: preparation, characterization, and optical, dielectric properties", *Polymer*, **55** (2014), 3634–3641.
36. H.T. Vo, F.G. Shi, "Towards model-based engineering of optoelectronic packaging material: dielectric constant modeling", *Microelectron. J.*, **33** (2002), 409–415.
37. X. Shi, H. Lian, X. Yan, R. Qi, N. Yao, T. Li, "Fabrication and properties of polyimide composites filled with zirconium tungsten phosphate of negative thermal expansion", *Mater. Chem. Phys.*, **179** (2016) 72–79.

38. Y. Ma, Q. Zhang, K. Zhao, C. Liu, B. Zhang, X. Zhang, Y. Zhoua, "Tunable negative thermal expansion of ultralight ZrW_2O_8/graphene hybrid metamaterial", *Carbon*, **153** (2019) 32–39.

39. Z.H. Shui, R. Zhang, W. Chen, D. Xuan, "Effects of mineral admixtures on the thermal expansion properties of hardened cement paste", *Constr. Build. Mater.*, **24** (2010) 1761–1767.